



Degradation of WTAP blocks antiviral responses by reducing the m⁶A levels of IRF3 and IFNAR1 mRNA

Yong Ge^{1,2,†}, Tao Ling^{1,2,†}, Yao Wang^{1,3}, Xin Jia^{1,4}, Xiongmei Xie¹, Rong Chen^{1,2}, Shangwu Chen¹, Shaochun Yuan^{1,2,5,*}  & Anlong Xu^{1,3,**} 

Abstract

N⁶-methyladenosine (m⁶A) is a chemical modification present in multiple RNA species and is most abundant in mRNAs. Studies on m⁶A reveal its comprehensive roles in almost every aspect of mRNA metabolism, as well as in a variety of physiological processes. Although some recent discoveries indicate that m⁶A can affect the life cycles of numerous viruses as well as the cellular antiviral immune response, the roles of m⁶A modification in type I interferon (IFN-I) signaling are still largely unknown. Here, we reveal that WT1-associated protein (WTAP), one of the m⁶A “writers”, is degraded via the ubiquitination-proteasome pathway upon activation of IFN-I signaling. With the degradation of WTAP, the m⁶A levels of IFN-regulatory factor 3 (*IRF3*) and interferon alpha/beta receptor subunit 1 (*IFNAR1*) mRNAs are reduced, leading to translational suppression of *IRF3* and instability of *IFNAR1* mRNA. Thus, the WTAP-*IRF3*/*IFNAR1* axis may serve as negative feedback pathway to fine-tune the activation of IFN-I signaling, which highlights the roles of m⁶A in the antiviral response by dictating the fate of mRNAs associated with IFN-I signaling.

Keywords antiviral responses; *IFNAR1*; *IRF3*; m⁶A modification; WTAP

Subject Categories Immunology; Microbiology, Virology & Host Pathogen Interaction; RNA Biology

DOI 10.15252/embr.202052101 | Received 16 November 2020 | Revised 15 August 2021 | Accepted 17 August 2021 | Published online 1 September 2021

EMBO Reports (2021) 22: e52101

Introduction

Type I interferons (IFN-Is) have vital roles in antiviral innate immunity. After viral infection, germline-encoded pattern recognition receptors (PRRs), such as Toll-like receptors (TLRs), RIG-I-like receptors (RLRs), NOD-like receptors (NLRs), and C-type lectin receptors (CLRs), can recognize nucleic acids derived from viruses,

leading to activation of *IRF3*, *IRF7*, and nuclear factor- κ B (NF- κ B) to induce the production of IFN-I (Yan & Chen, 2012; Schlee & Hartmann, 2016). The secreted type I interferons (IFN α/β) then bind to the heterodimeric receptor complex composed of two chains (*IFNAR1* and *IFNAR2*), which amplify and spread the antiviral response to surrounding uninfected cells via the Janus kinase/signal transducer and activator of transcription (Jak-STAT) signaling pathway (Villarino *et al.*, 2017). Activation of the Jak-STAT pathway results in the transcription of hundreds of interferon-stimulated genes (ISGs), most of which encode products with profound antiviral effects, thus establishing an innate immune state against invading pathogens and maintaining homeostasis (Schneider *et al.*, 2014; Barrat *et al.*, 2019).

Although IFN-I has critical roles in protection from pathogens, excessive IFN responses contribute to immune pathogenesis such as inflammatory autoimmune diseases and infectious diseases via aberrantly activating inflammation. Thus, to ensure the most favorable outcome, the host has developed sophisticated mechanisms at multiple levels to maintain appropriate IFN responses. For example, almost all ISGs are rich in ISRE (interferon-sensitive response element) motifs, and their transcription is initiated when the Jak-STAT signaling is activated (Levy *et al.*, 1988). When the translational repressors 4E-BP1 and 4E-BP2 are lacking, the threshold for eliciting IFN-I production is lowered (Colina *et al.*, 2008). In addition to transcriptional and translational regulation of many ISGs, the activation of IFN-I can be tightly regulated at the post-translational level. For instance, the activity and stability of many key components involved in IFN-I activation, such as the sensors RIG-I and cGAS, can be regulated by ubiquitination and deubiquitylation (Gack *et al.*, 2007; Chen & Chen, 2019; Tao *et al.*, 2020; Zhang *et al.*, 2020). The activation of some key adaptors, such as MAVS, STING, and TRIF, is regulated by phosphorylation at their conserved pLxIS (p, hydrophilic residue; x, any residue; S, phosphorylation site) motif (Liu *et al.*, 2015).

Recently, a new epigenetic modification, N⁶-methyladenosine (m⁶A), has aroused extensive attention. m⁶A is the most prominent

1 Guangdong Province Key Laboratory of Pharmaceutical Functional Genes, MOE Key Laboratory of Gene Function and Regulation, State Key Laboratory of Biocontrol, School of Life Sciences, Sun Yat-Sen University, Guangzhou, China

2 Southern Marine Science and Engineering Guangdong Laboratory (Zhuhai), Zhuhai, China

3 School of Life Sciences, Beijing University of Chinese Medicine, Beijing, China

4 School of Chinese Materia Medica, Beijing University of Chinese Medicine, Beijing, China

5 Laboratory for Marine Biology and Biotechnology, Pilot National Laboratory for Marine Science and Technology, Qingdao, China

*Corresponding author. Tel: +86 20 39332956; E-mail: yuanshch@mail.sysu.edu.cn

**Corresponding author. Tel: +86 20 39332990; E-mail: lssxl@mail.sysu.edu.cn

†These authors contributed equally to the work

mRNA modification in higher eukaryotes, governed by methyltransferase complex (“writers”), demethylases (“erasers”), and RNA-binding proteins (“readers”) (Roignant & Soller, 2017; Frye *et al*, 2018). m⁶A is added to mRNA by a multisubunit “writer” complex composed of the METTL3/METTL14/WTAP heterotrimer and many additional adaptor proteins. METTL3 is the enzymatic component of the complex, and METTL14 is an allosteric activator that also binds to the target RNA. In this heterotrimer, WTAP is essential for m⁶A deposition and helps the METTL3-METTL14 heterodimer localize to transcription sites (Ping *et al*, 2014; Śledź & Jinek, 2016). m⁶A modification has been linked to various stages along the posttranscriptional trajectory of mRNA and, in particular, to promotion of mRNA splicing, export, decay, translation, and subcellular localization (Wang *et al*, 2014, 2015; Meyer & Jaffrey, 2017). Functionally, m⁶A has been shown to impact fundamental cellular processes in diverse organisms, including meiosis, the circadian clock, DNA damage repair, and the stress response (Xiang *et al*, 2017; Xu *et al*, 2017; Fustin *et al*, 2018; Zhou *et al*, 2018). Studies also show that different expression levels, post-translational modifications (PTMs), and cellular localization of “writer” proteins, depending on cell type and/or in response to environmental stimuli, can regulate the processing of m⁶A and provide unique potential to tune gene expression in different biological processes (Wang *et al*, 2016; Xiang *et al*, 2017; Du *et al*, 2018). In short, the role of m⁶A in regulating mRNA fate and its functional importance in various cell types have been widely studied. Recently, some studies have suggested that m⁶A may also be involved in regulation of host immunity as well as viral replication (Zheng *et al*, 2017; Winkler *et al*, 2019). However, the specific mechanisms, especially whether and how m⁶A modification tightly regulates IFN-I signaling, are still unclear.

In this study, we report that WTAP, one of the m⁶A “writer” proteins, is depleted via ubiquitination-proteasome-mediated degradation upon viral infection. Degradation of WTAP leads to reduced m⁶A methylation of *IRF3* and *IFNAR1* mRNAs, resulting in translational suppression of *IRF3* and mRNA instability of *IFNAR1*. Thus, the precise control of *IRF3* and *IFNAR1* by m⁶A modification fine-tunes the antiviral responses to protect the host from immunopathology of over-reactive and harmful IFN-I production. In brief, our findings highlight WTAP as a regulator involved in antiviral immunity, providing a novel diagnostic marker and therapeutic target for related immune diseases.

Results

WTAP protein is decreased in virus-infected or nucleic acid analog-treated cells

From previous studies, m⁶A is added to mRNA by a multisubunit writer complex, and the most important of which is the METTL3/METTL14/WTAP heterotrimer. The protein abundance of these writers can regulate m⁶A modification and control biological processes. To investigate the role of m⁶A modification in regulation of the IFN-I signaling pathway, we first analyzed the expression of the key m⁶A writer proteins-METTL3, METTL14, and WTAP in PBMCs (peripheral blood mononuclear cells) upon viral infection or nucleic acid analog stimulation. The results showed that, along with upregulation of RIG-I or MDA5, the protein level of WTAP was

significantly decreased when PBMCs were challenged with VSV-eGFP (vesicular stomatitis virus with enhanced GFP), intracellular poly(I:C) LMW (low molecular weight), HSV-1 (herpes simplex virus 1), or intracellular HSV-60 (synthetic herpes simplex virus 1 DNA analog). However, as the key enzymatic components, the protein abundances of METTL3 and METTL14 were slightly changed only when PBMCs were challenged with poly(I:C) or HSV-60 (Fig 1A). Subsequently, the same treatments were performed in BMDMs (mouse bone marrow-derived macrophages) and similar results were obtained. The protein level of WTAP was significantly decreased with all indicated treatments in BMDMs, while METTL14 exhibited a downward trend only with poly(I:C) (LMW) or HSV-60 stimulation (Fig 1B). Then, we further validated the above phenotypes in human and mouse cell lines, such as A549, L929, and MEF (mouse embryonic fibroblast) cells. We also found that the protein abundance of WTAP, but not of METTL3 or METTL14, was reduced in A549 and L929 cells infected with VSV or SeV (Sendai virus) (Figs 1C and EV1A), or transfected with poly(I:C) (LMW) or poly(dA:dT) (Figs 1D and EV1B). In addition, WTAP was also significantly decreased in A549 cells (Fig EV1C) and MEFs (Fig EV1D) infected with HSV-1. However, the protein levels of METTL3 and METTL14 were not changed significantly upon the same treatments. Overall, the protein abundance of WTAP gradually decreased upon activation of IFN-I signaling after viral infection or nucleic acid analog treatment, while no uniform or broad trend in METTL3 and METTL14 expression was observed. These results indicate a potential relationship between m⁶A modification and the regulation of IFN-I signaling, in which WTAP may be an important regulator.

WTAP is degraded through the K48-linked ubiquitination-proteasome pathway upon activation of IFN-I signaling

It is well known that protein abundance is mainly regulated by transcriptional and post-translational modifications. To explore what affects the protein abundance of WTAP upon activation of IFN-I signaling, we first detected the transcriptional changes of WTAP. The results showed that the transcription of *WTAP* was slightly activated by both viral infections (VSV-eGFP or HSV-1) and nucleic acid analog treatments (poly(I:C), poly(dA:dT) or HSV-60) in PBMCs, BMDMs, and A549 cells (Fig 2A–C). However, stimulation with IFN- α or IFN- β in A549 cells (Fig 2D) and BMDMs (Fig EV2A) had no effect on the mRNA abundance of *WTAP*. These data indicate that the degradation of WTAP may be caused by post-translational modification instead of transcriptional regulation upon activation of IFN-I signaling.

It has been documented that WTAP can undergo degradation depending on the ubiquitin-proteasome pathway (Kuai *et al*, 2018). To explore whether WTAP is degraded when activating IFN-I signaling, the protein abundance of WTAP in the presence of the proteasome inhibitors carfilzomib (PR-171) and bortezomib (PS-341) or autophagy inhibitors chloroquine (CQ) and bafilomycin A1 (Baf A1) was tested. PR-171 is an irreversible proteasome inhibitor, while PS-341 is a reversible inhibitor of the proteasome (Fricker, 2020), and both are commonly used in clinical treatment and scientific research. The results showed that PR-171 and PS-341 (Figs 2E and EV2B), but not CQ and Baf A1 (Figs 2F and EV2C), blocked the VSV-eGFP- or nucleic acid analog-mediated degradation of WTAP in A549 cells. In addition, higher levels of ubiquitinated WTAP were observed in the presence of PR-171 than in the presence of DMSO

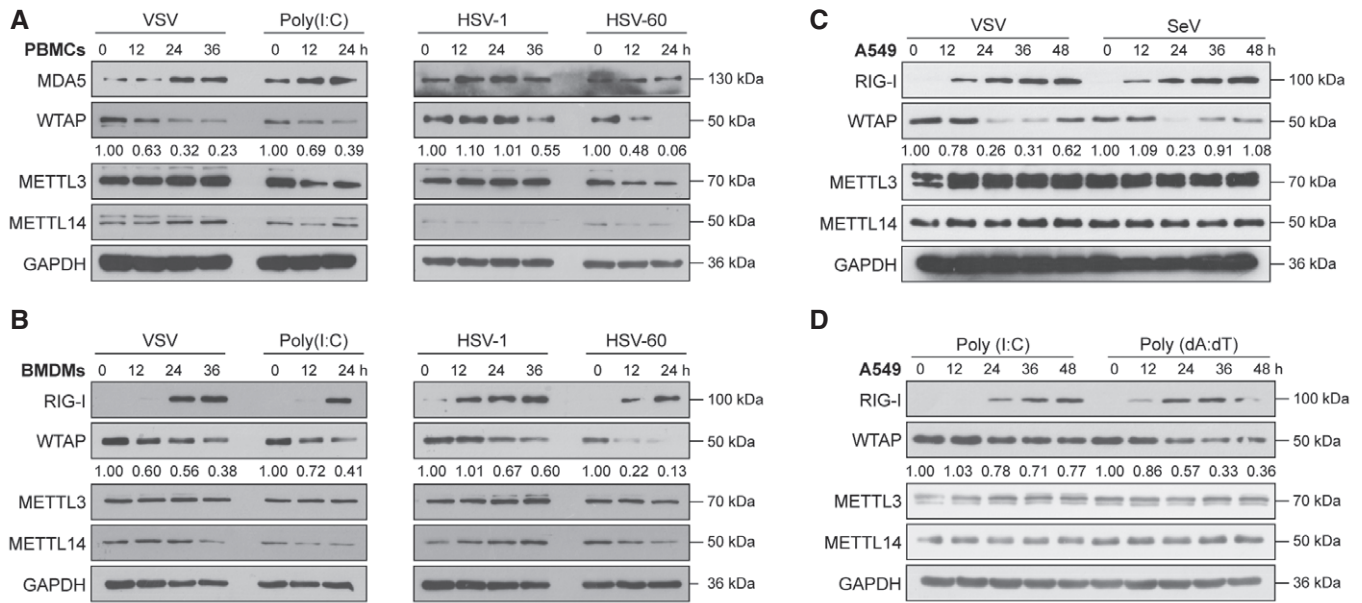


Figure 1. WTAP protein is decreased in virus-infected or nucleic acid analog-treated cells.

A, B Immunoblot analyses of the protein abundance of the METTL3/METTL14/WTAP heterotrimer in PBMCs (A) and BMDMs (B) upon challenge with VSV-eGFP, poly(I:C), HSV-1, or HSV-60 at the indicated time points. Data are representative of three independent biological experiments.

C, D Immunoblot analyses of the protein abundance of the METTL3/METTL14/WTAP heterotrimer in A549 cells upon challenge with VSV-eGFP or SeV (C) and poly(I:C) or poly(dA:dT) (D) at the indicated time points. Data are representative of three independent biological experiments.

Source data are available online for this figure.

(Fig 2G), revealing that WTAP undergoes ubiquitination upon viral infection. To determine what type of ubiquitin chain is added to WTAP, we transfected 293T cells with Flag-tagged WTAP together with HA-tagged K48-linked ubiquitin (K48-Ub), K63-linked ubiquitin (K63-Ub), or wild-type ubiquitin (HA-Ub), and found that WTAP undergoes both K48-linked and K63-linked ubiquitination. However, only K48-linked, but not K63-linked ubiquitination of WTAP, was markedly increased in the presence of the proteasome inhibitor PR-171 (Figs 2H and EV2D). All these results suggest that K48-linked

ubiquitination-proteasomal degradation is the main reason for the decrease of WTAP protein upon activation of IFN-I signaling.

WTAP positively regulates the antiviral immune responses

To determine the relationship between WTAP and the activation of IFN-I signaling, we first knocked out WTAP using CRISPR-Cas9 systems (Ran *et al*, 2013) in A549, L929, and 293T cells. However, only one *WTAP*^{-/-} 293T subclone was obtained after a series of

Figure 2. WTAP is degraded through the K48-linked ubiquitination-proteasome pathway upon the activation of IFN-I signaling.

A, B Real-time PCR (qRT-PCR) analyses of *WTAP* mRNA expression in PBMCs (A) or BMDMs (B) upon challenge with VSV-eGFP, poly(I:C), HSV-1, or HSV-60 at indicated time points. $n = 3$ independent biological replicates, and error bars represent standard deviations. Data were compared using Student's *t*-test.

C qRT-PCR analyses of *WTAP* mRNA expression in A549 cells upon challenge with VSV-eGFP, poly(I:C), HSV-1, or poly(dA:dT) at the indicated time points. $n = 3$ independent biological replicates, and error bars represent standard deviations. Data were compared using Student's *t*-test.

D qRT-PCR analyses of *WTAP* mRNA expression in A549 cells stimulated with IFN- α or IFN- β at the indicated time points. $n = 3$ independent biological replicates, and error bars represent standard deviations. Data were compared using Student's *t*-test.

E A549 cells were stimulated with poly(I:C) for 16 h and then treated with PR-171 (10 μ M) or PS-341 (10 μ M) for additional 4 and 8 h. The cell lysates were analyzed by immunoblotting. Representative images from three independent biological experiments are shown (left), and the relative levels of WTAP are presented as the mean \pm SD (right).

F A549 cells were stimulated with poly(I:C) for 16 h and then treated with CQ (50 mM) or Baf A1 (0.2 mM) for additional 4 and 8 h. The cell lysates were analyzed by immunoblotting. LC3B served as a good marker of the autophagy process. Representative images from three independent biological experiments are shown (left), and the relative levels of WTAP are presented as the mean \pm SD (right).

G Immunoassays of extracts of A549 cells infected with VSV-GFP for 16 h and then treated with PR-171 (10 μ M) or DMSO for additional 4 and 8 h, followed by immunoprecipitation with anti-WTAP antibody and immunoblot analysis with anti-Ub antibody. Data are representative of three independent biological experiments.

H Coimmunoprecipitation and immunoblot analyses of extracts of 293T cells transfected with various combinations of plasmids encoding FLAG-tagged WTAP, and HA-tagged K48-linked, K63-linked or wild-type ubiquitin and treated with DMSO or PR-171 (10 μ M). Data are representative of three independent biological experiments.

Source data are available online for this figure.

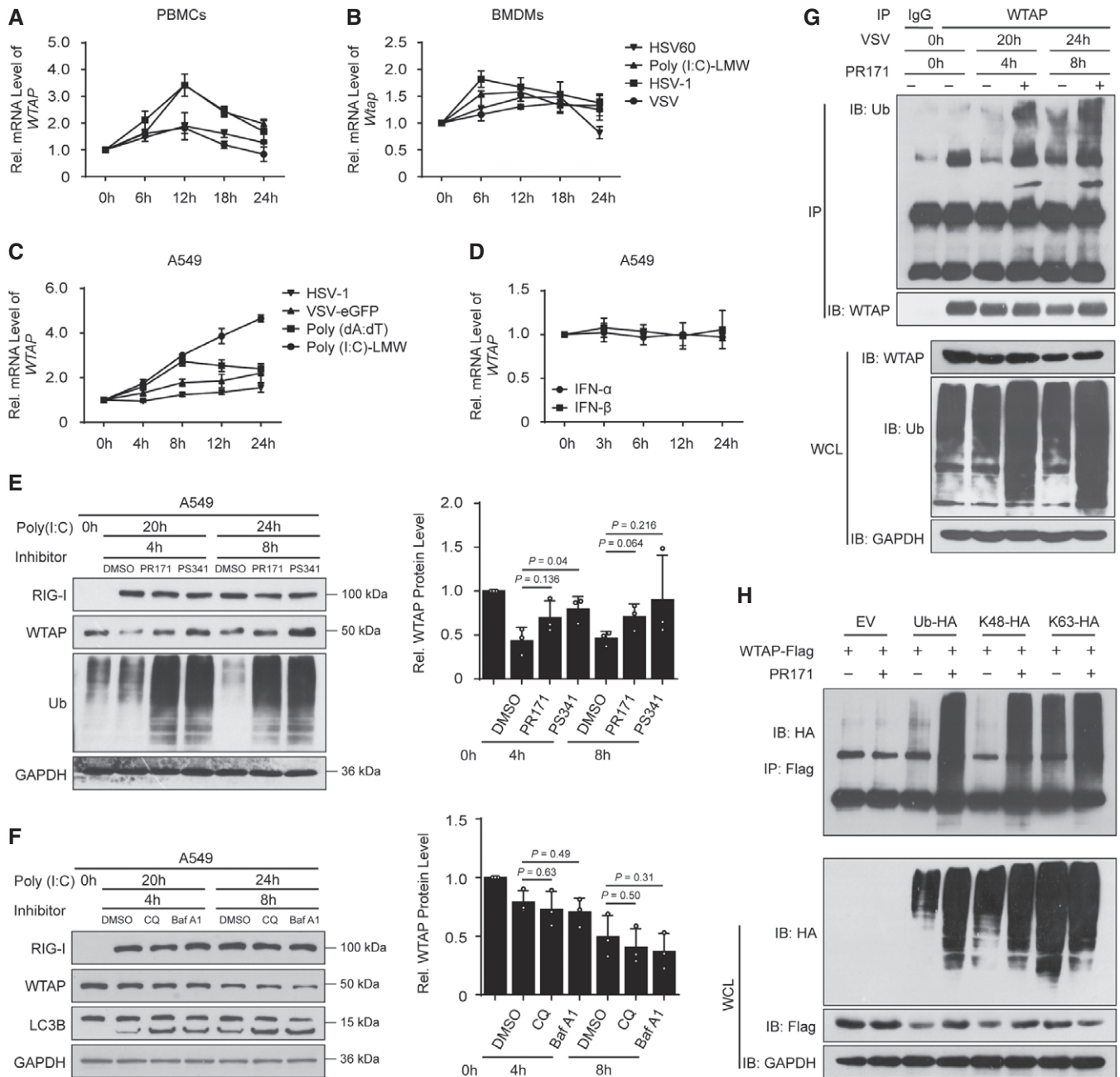


Figure 2.

efforts (Fig 3A). We then used this subclone to investigate the role of WTAP in IFN- β production via dual-luciferase assays. The results showed that the activities of IFN- β promoter-based luciferase reporter (IFN- β -luc) and interferon-stimulated response element (ISRE)-based luciferase reporter were upregulated upon viral infection in 293T cells. However, when endogenous WTAP was knocked out, the increased IFN- β -luc and ISRE-luc activities mediated by VSV-eGFP infection or poly(I:C) and poly(dA:dT) stimulation were significantly reduced (Fig 3B). Such defects could be rescued in a dose-dependent manner when exogenous WTAP was overexpressed

in *WTAP*^{-/-} 293T cells infected with VSV-eGFP or treated with poly(I:C) or poly(dA:dT) (Fig EV3A–C). Similarly, decreased mRNA abundances of *IFNB1*, *RANTES*, *DDX58*, and *ISG15* were observed in *WTAP*^{-/-} 293T cells upon VSV-eGFP, poly(I:C), or poly(dA:dT) treatments (Fig 3C). These data indicate a positive regulation mediated by WTAP in the IFN-I signaling pathway.

Since no *WTAP*^{-/-} A549 subclones were obtained in this study, we had to design WTAP-specific small interfering RNA (siRNA) and short hairpin RNA (shRNA) to efficiently knockdown the expression of WTAP in A549 cells to further investigate the role of WTAP in

regulating antiviral immune responses (Fig 3D and EV3D and E). Consistent with the observations in *WTAP*^{-/-} 293T cells, induced mRNA expression of *IFNB1* (Figs 3E and EV3F), *RANTES*, and *ISG15* (Figs 3F and EV3G) after poly (I:C)-HMW, poly (I:C)-LMW, or poly (dA:dT) treatments was decreased in *WTAP* knockdown A549 cells. The average size of poly(I:C)-LMW ranges from 0.2 to 1 kb, while that of poly(I:C)-HMW ranges from 1.5 to 8 kb. The LMW form is mainly recognized by retinoic acid-inducible protein I (RIG-I), while the HMW form is mainly recognized by melanoma differentiation-associate gene 5 (MDA5) (Kato et al, 2006). Moreover, the secretion of IFN- β (Figs 3G and EV3H) and CCL5 (Figs 3H and EV3I) was also significantly reduced in *WTAP* knockdown A549 cells upon stimulation. We also observed a decrease in the protein levels of ISGs (RIG-I, MDA5, Mx1, and IFIT2) in sh*WTAP* A549 cells that were stimulated with poly I:C (LMW) or poly dA:dT (Fig 3I and J). Conversely,

the overexpression of exogenous *WTAP* in A549 cells following treatment with poly (I:C) or poly (dA:dT), not only increased the mRNA transcription of *IFNB1* (Figs 3K and EV3J) and *RANTES* (Figs 3L and EV3K), but also promoted the secretion of IFN- β (Figs 3M and EV3L) and CCL5 (Figs 3N and EV3M). The overexpression of *WTAP* also increased the protein abundance of ISGs after poly (I:C) or poly (dA:dT) stimulation (Fig EV3N) in A549 cells. Taken together, these results strongly suggest that *WTAP* is important for activation and preservation of IFN-I signaling.

WTAP regulates the antiviral responses by targeting both IFN-I and Jak-STAT signaling

Following detection of viral invasion, the transcription factors IRF3 and IRF7 are phosphorylated by TBK1 and then translocate into the

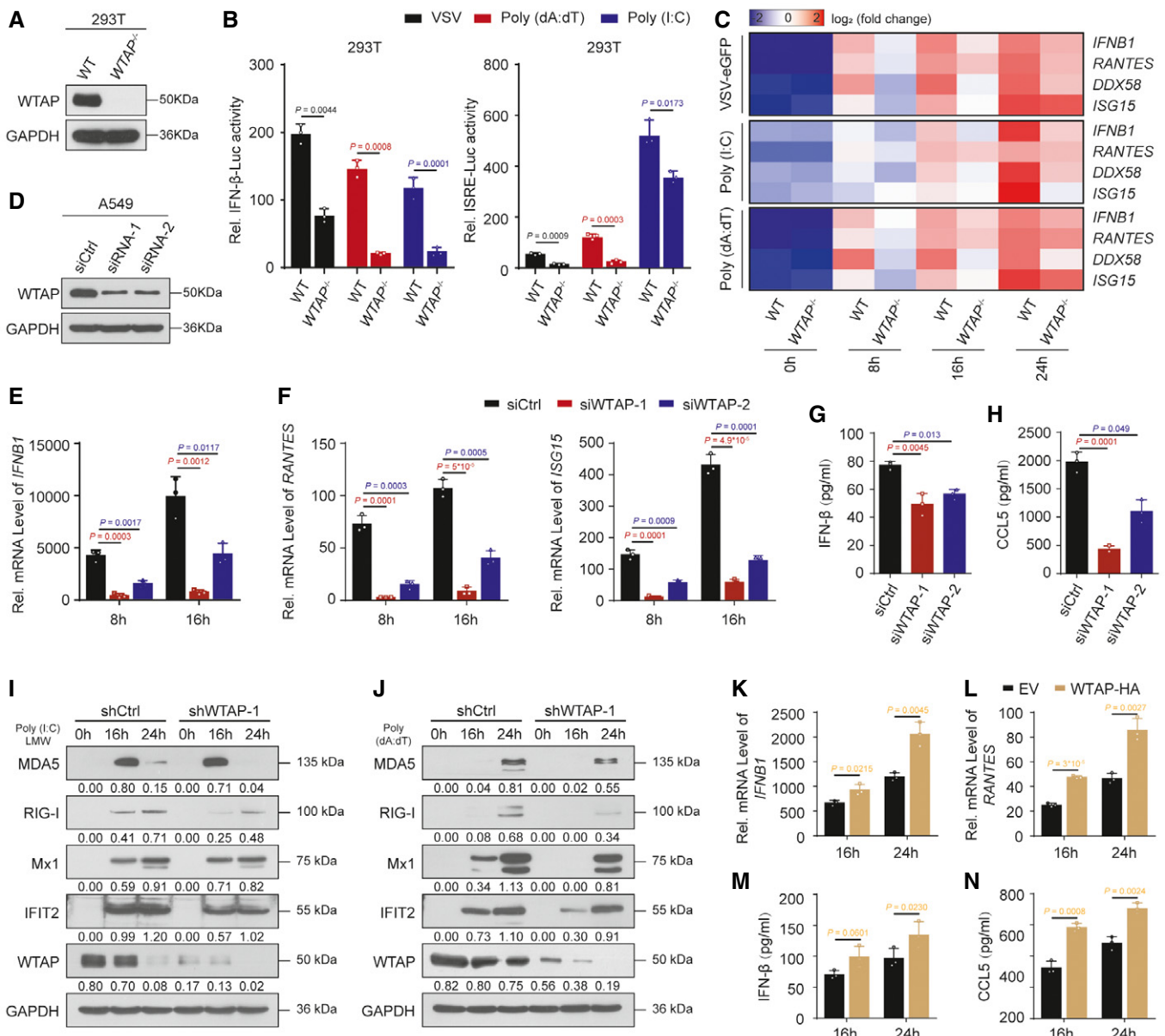


Figure 3.

Figure 3. WTAP positively regulates the antiviral immune responses.

- A WTAP knockout efficiency in 293T cells detected by immunoblotting. Data are representative of three independent biological experiments.
- B Luciferase activity analyses in wild-type (WT), or *WTAP*^{-/-} 293T cells, transfected with a luciferase reporter for IFN- β (IFN- β -luc) or ISRE (ISRE-luc) followed by treatments with intracellular poly(I:C), poly(dA:dT), or VSV-eGFP. The results are expressed relative to Renilla luciferase activity. $n = 3$ independent biological replicates, and error bars represent standard deviations. Data were compared using Student's t -test.
- C qRT-PCR analyses to detect the mRNA abundances of *IFNB1*, *RANTES*, *DDX58*, and *ISG15* in WT and *WTAP*^{-/-} 293T cells followed by treatments with intracellular poly(I:C), poly(dA:dT), or VSV-eGFP. Data are representative of three independent biological experiments.
- D Immunoblot analyses to detect the WTAP knockdown efficiency in A549 cells after transfection with Ctrl or WTAP-specific siRNAs for 48 h. Data are representative of three independent biological experiments.
- E, F qRT-PCR analyses to detect the mRNA abundance of *IFNB1* (E), *RANTES*, and *ISG15* (F) in A549 cells transfected with Ctrl or WTAP-specific siRNA, followed by treatment with poly(I:C)-HMW at the indicated time points. $n = 3$ independent biological replicates, and error bars represent standard deviations. Data were compared using Student's t -test.
- G, H ELISA analyses to detect IFN- β (G) and CCL5 (H) secretion in supernatants from E at 16 h. $n = 3$ independent biological replicates, and error bars represent standard deviations. Data were compared using Student's t -test.
- I, J Immunoblot analyses to detect the protein expression of ISGs in shCtrl and shWTAP A549 cells that were stimulated with poly(I:C)-LMW (I) or poly(dA:dT) (J) at different time points with the indicated antibodies. Data are representative of three independent biological experiments.
- K, L qRT-PCR analyses to detect the mRNA abundances of *IFNB1* (K) and *RANTES* (L) in A549 cells transfected with empty vector (EV) or WTAP-HA plasmid, followed by treatment with poly(I:C)-HMW at the indicated time points. $n = 3$ independent biological replicates, and error bars represent standard deviations. Data were compared using Student's t -test.
- M, N ELISA analyses to detect IFN- β (M) and CCL5 (N) secretion in supernatants from K. $n = 3$ independent biological replicates, and error bars represent standard deviations. Data were compared using Student's t -test.

Source data are available online for this figure.

nucleus to activate the transcription and production of IFN-I. Secreted IFN-I then binds to surface receptors to regulate the transcription of hundreds of ISGs through Jak-STAT signaling (Villarino *et al*, 2017). To determine how WTAP affects the production of IFNs and the transcription of ISGs, we first detected whether WTAP knockdown affects the phosphorylation of IRF3 and TBK1 upon nucleic acid analog treatment or viral infection. The results showed that phosphorylated and total IRF3, but not TBK1, were significantly decreased in WTAP knockdown A549 cells upon poly (I:C) or poly (dA:dT) stimulation (Fig 4A and B), as well as upon VSV-eGFP, SeV, or HSV-1 infection (Fig EV4A–C). Similarly, the dimerization of IRF3 induced by poly (I:C) or poly (dA:dT) (Fig 4C) or VSV-eGFP or SeV (Fig EV4D) was impaired in WTAP knockdown A549 cells. In addition, WTAP knockdown A549 cells produced fewer ISGs than control cells after stimulation with IFN- α or IFN- β (Fig 4D). Consistent with the decrease in ISG production, the phosphorylation of STAT1 was decreased considerably in shWTAP A549 cells in response to treatment with IFN- α (Fig 4E) or IFN- β (Fig 4F). Thus, WTAP may affect the upstream type I signaling response, as well as the downstream Jak-STAT pathway.

WTAP maintains the protein abundance of IRF3 and IFNAR1 through m⁶A modification

To determine the molecular targets of WTAP, we next tested whether the protein abundances of the identified key components involved in IFN-I signaling were changed in WTAP knockdown A549 cells. We found that the protein abundances of IRF3 and IFNAR1 but not of the other tested proteins were impaired in WTAP knockdown A549 cells (Fig 5A and B). Moreover, no significant changes in IRF3 and IFNAR1 proteins were observed in METTL3- or METTL14-knockdown A549 cells (Fig EV4E). These results suggest that WTAP may specifically maintain the protein abundances of IRF3 and IFNAR1 to participate in antiviral immune responses.

WTAP is one of the subunits of the methyltransferase complex (“writer”) and is required for anchoring of methyltransferase

complexes in nuclear speckles, which is where methylation occurs. Recent studies have shown that the depletion of WTAP results in significantly lower m⁶A levels in global or specific mRNAs (Ping *et al*, 2014; Chen *et al*, 2019). As expected, the level of m⁶A methylation was substantially decreased in WTAP knockdown A549 cells compared with control cells (Figs 5C and EV4F). Thus, we next analyzed whether WTAP regulates IRF3 and IFNAR1 expression in an m⁶A-dependent manner. First, we used RMBase v2.0 to predict the m⁶A sites with “DRACH” elements in *IRF3* and *IFNAR1* transcripts (Xuan *et al*, 2018) and found that most of the m⁶A modification sites with high confidence were distributed near the 5'-untranslated regions (5'-UTRs) of *IRF3* and 3'-untranslated regions (3'-UTRs) of *IFNAR1* transcripts. To elucidate the function of WTAP in the m⁶A modification of *IRF3* and *IFNAR1* transcripts, we designed two gene-specific primer pairs, F1/R1 and F2/R2, to detect the change of m⁶A modification levels at site 1 and site 2 of these two genes using MeRIP-qPCR assays (Fig 5D and E). The results showed that m⁶A-modified *IRF3* and *IFNAR1* transcripts were effectively enriched by m⁶A-specific antibody. Enriched m⁶A modifications at site 1 but not site 2 of *IRF3* and *IFNAR1* were remarkably decreased in WTAP knockdown A549 cells (Fig 5F and G), but increased in WTAP-overexpressing A549 cells (Figs 5H and EV4G). In addition, although the enriched m⁶A modifications at site 1 and site 2 of *IFNAR1* transcripts were remarkably decreased in siMETTL3 A549 cells (Fig EV4H), only m⁶A modifications at site 1 of *IRF3* transcripts were significantly reduced (Fig EV4I). Due to the limitations of MeRIP-PCR assays, which cannot distinguish single site changes in target genes, we next performed a statistical analysis of the published m⁶A-seq dataset (GSE55572) to further explore the contributions of WTAP or METTL3/METTL14 to the m⁶A modification of *IRF3* and *IFNAR1* transcripts (Data ref: Schwartz *et al*, 2014). The results showed that the depletion of WTAP had a larger effect on the m⁶A modifications of *IFNAR1* and *IRF3* transcripts than the depletion of METTL3 or METTL14 (Fig EV4J and K). Among the three identified m⁶A peaks in the 3'UTR near the stop codon of *IFNAR1* transcripts, METTL3 and METTL14 specifically affected the

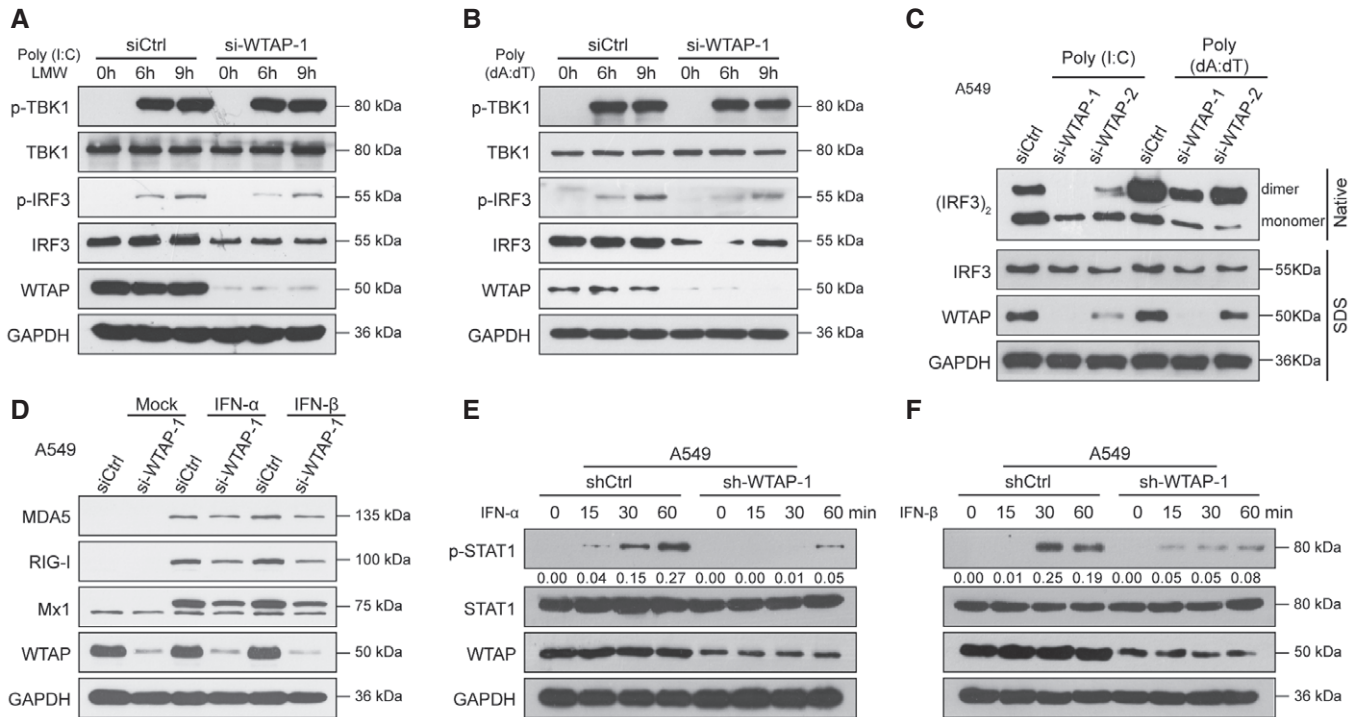


Figure 4. WTAP regulates the antiviral responses by targeting both IFN-I and Jak-STAT signaling.

A, B Immunoblot analyses of total and phosphorylated (p-) TBK1 and IRF3 in A549 cells transfected with Ctrl or WTAP-specific siRNA, followed by stimulation with poly (I:C) (A) or poly (dA:dT) (B) at different time points. Data are representative of three independent biological experiments.

C Immunoblot analyses of IRF3 dimerization in A549 cells transfected with Ctrl or WTAP-specific siRNA, followed by stimulation with poly (I:C) or poly (dA:dT) for 6 h. Data are representative of three independent biological experiments.

D Immunoblot analyses to detect the protein expression of ISGs in A549 cells transfected with Ctrl or WTAP-specific siRNA, followed by stimulation with IFN- α or IFN- β (50 U/ml) for 4 h. Data are representative of three independent biological experiments.

E, F Immunoblot analyses of total and phosphorylated (p-) STAT1 in shCtrl and shWTAP A549 cells, followed by stimulation with IFN- α (E) or IFN- β (F) at different time points. Data are representative of three independent biological experiments.

Source data are available online for this figure.

site of peak 2, while WTAP was more sensitive to the sites of peaks 1 and 3 (Fig EV4J). Moreover, both m⁶A peaks identified in the 5'UTR of *IRF3* transcripts were affected by WTAP depletion, while only peak 2 was affected in siMETTL3 or siMETTL14 cells (Fig EV4K). Thus, although WTAP cannot methylate mRNAs in the absence of METTL3, we hypothesized that WTAP is required to bring the “writer” complexes to the target mRNAs at some m⁶A sites and ultimately affects the fate of target genes. Moreover, as Chelmicki showed (Chelmicki *et al.*, 2021), we also observed an increased WTAP protein abundance in METTL3 and METTL4 knockdown cells (Fig EV4E), indicating that the increase in WTAP protein may offset the effect of METTL3 or METTL4 defects on *IRF3* and *IFNAR1*.

m⁶A methylation can affect many aspects of gene expression, including nuclear export, mRNA decay, alternative pre-mRNA splicing, 3' end processing, and translation (Roundtree *et al.*, 2017). We first evaluated the mRNA abundance of *IRF3* and *IFNAR1* in WTAP knockdown A549 cells and found that only *IFNAR1* was significantly downregulated (Figs 5I and EV5A). Subsequent experiments showed that the nuclear export of *IRF3* and *IFNAR1* (Figs 5J and EV5B and C) was not affected when WTAP was knocked down in A549 cells. Thus, we next explored whether WTAP-mediated

methylation is implicated in *IRF3* and *IFNAR1* mRNA decay. In fact, when transcription was halted with actinomycin D (Act D), the decay rate of *IFNAR1* but not *IRF3* mRNA was considerably faster in WTAP knockdown A549 cells (Figs 5K and EV5D and E). Consistently, the rate of *IFNAR1* protein reduction was also faster in WTAP knockdown A549 cells (Fig 5L) after treatment with Act D. Since WTAP did not affect the decay rate of *IRF3* mRNA, we investigated whether WTAP-mediated methylation is implicated in the translation efficiency of *IRF3* and *IFNAR1* mRNAs through polysome profiling. We calculated the proportion of mRNAs in polysome fractions measured by qRT-PCR and found that the distribution of *IRF3* but not *IFNAR1* mRNA shifted to the lighter fraction in WTAP knockdown cells (Figs 5M and EV5F), and this difference was not caused by RNA loss during RNA extraction (Fig EV5G). To determine whether the effect on *IRF3* and *IFNAR1* transcripts is directly caused by WTAP, we first mutated the putative m⁶A-modified adenosines to thymines in *IRF3* and *IFNAR1* mRNAs and inserted these mutated UTRs into a reporter gene plasmid (psiCHECKTM-2) (Fig 5N and O). Then, luciferase reporter assays were performed, and the results showed that the luciferase activities of the reporter constructs bearing the *IFNAR1*-3' UTR or *IRF3*-5' UTR with mutations (Mut) at m⁶A sites were significantly weaker than those

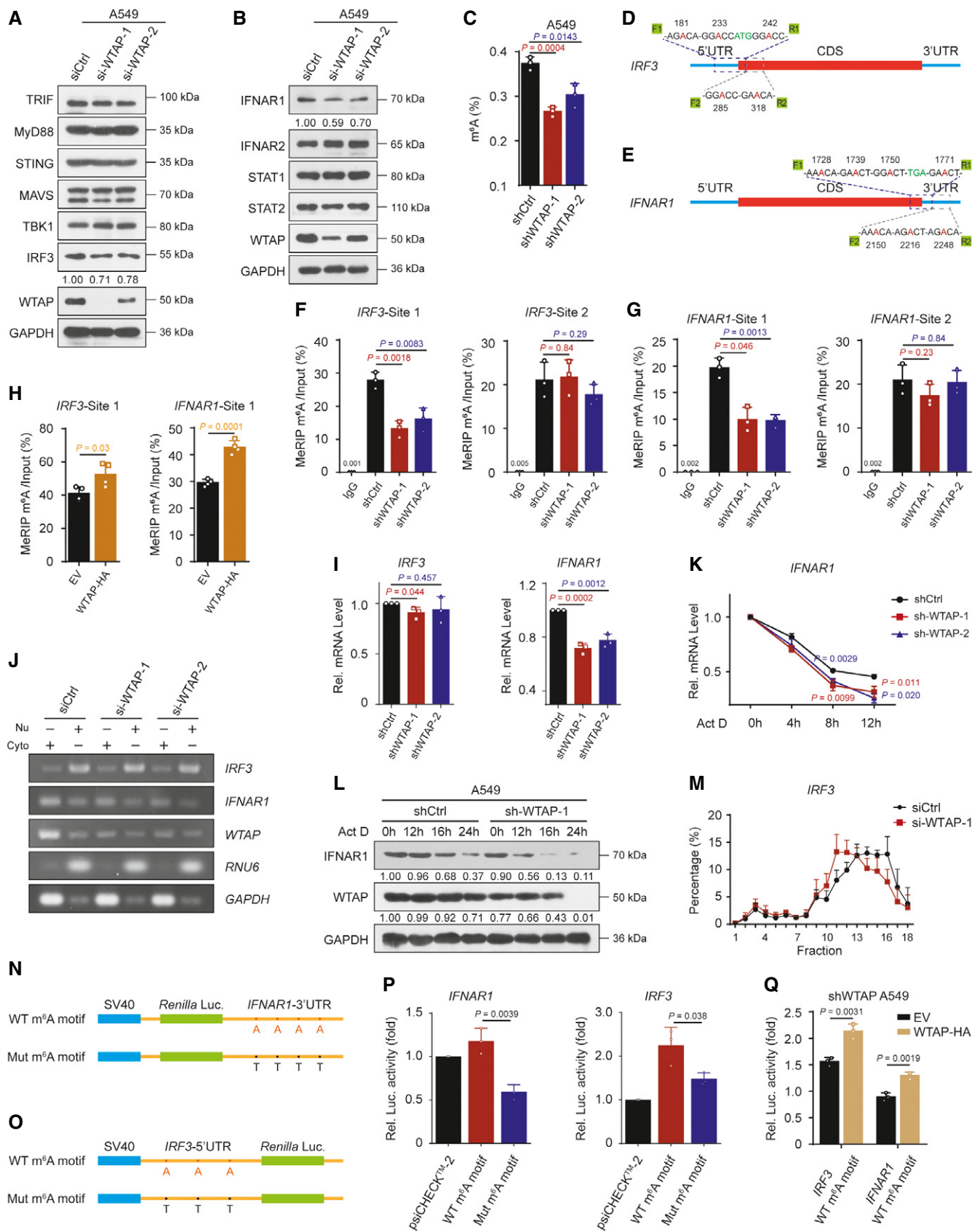


Figure 5.

Figure 5. WTAP maintains the protein abundance of IRF3 and IFNAR1 through m⁶A modification.

- A, B Immunoblot analyses to detect the protein expression of critical adaptors in the IFN-I and Jak-STAT signaling pathway in A549 cells after transfection with Ctrl or WTAP-specific siRNAs for 48 h. Data are representative of three independent biological experiments.
- C ELISA quantification of m⁶A levels in mRNA extracted from shCtrl and shWTAP A549 cells. *n* = 3 independent biological replicates, and error bars represent standard deviations. Data were compared using Student's *t*-test.
- D, E Schematic representation of the position of m⁶A motifs within the *IRF3* (D) and *IFNAR1* (E) transcripts. The sites of the m⁶A RNA modification element "DRACH" in *IRF3* mRNA 5'-UTRs or *IFNAR1* mRNA 3'-UTRs were predicted using RMBase v2.0 (<http://rna.sysu.edu.cn/rmbase/>). F1/R1 represents the detection site 1 containing three (*IRF3*) or four (*IFNAR1*) "DRACH" elements and F2/R2 represents the detection site 2 containing two (*IRF3*) or three (*IFNAR1*) "DRACH" elements.
- F, G Abundance of *IRF3* (F) and *IFNAR1* (G) transcripts (detection sites 1 and 2) among mRNA immunoprecipitated with anti-m⁶A antibody from shCtrl and shWTAP A549 cells. *n* = 3 independent biological replicates, and error bars represent standard deviations. Data were compared using Student's *t*-test.
- H Abundance of *IRF3* and *IFNAR1* transcripts (detection site 1) among mRNAs immunoprecipitated with anti-m⁶A antibody from A549 cells that were transfected with empty vector (EV) or HA-tagged WTAP plasmid for 24 h. *n* = 4 independent biological replicates, and error bars represent standard deviations. Data were compared using Student's *t*-test.
- I qRT-PCR analyses of the mRNA expression of *IRF3* and *IFNAR1* in shNC and shWTAP A549 cells. *n* = 3 independent biological replicates, and error bars represent standard deviations. Data were compared using Student's *t*-test.
- J Semi-qRT-PCR analyses of *IRF3* and *IFNAR1* mRNA and *RNU6* and *GAPDH* mRNA (loading controls throughout) in the nucleus (Nu) and cytoplasm (Cyto) of A549 cells transfected with Ctrl or WTAP-specific siRNA for 48 h. Data are representative of three independent biological experiments.
- K qRT-PCR analyses of *IFNAR1* mRNA expression in shCtrl and shWTAP A549 cells, followed by treatment with Act D (5 μg/ml) for the indicated times. *n* = 3 independent biological replicates, and error bars represent standard deviations. Data were compared using Student's *t*-test.
- L Immunoblot analyses of *IFNAR1* in shCtrl and shWTAP A549 cells, followed by treatment with Act D (5 μg/ml) for the indicated times. Data are representative of three independent biological experiments.
- M qRT-PCR analyses of the proportion of *IRF3* mRNA in polysome fractions from A549 cells transfected with Ctrl or WTAP-specific siRNAs. *n* = 3 independent biological replicates, and error bars represent standard deviations. Data were compared using Student's *t*-test.
- N, O Wild-type or mutated m⁶A consensus sequences (A-to-T mutation) of *IFNAR1*-3' UTR (N) and *IRF3*-5' UTR (O) were fused with Renilla luciferase reporter in psiCHECKTM-2 vector.
- P Relative luciferase activities in 293T cells after transfection with reporter vectors bearing *IFNAR1*-3' UTR or *IRF3*-5' UTR with wild-type (WT) or mutated (Mut) m⁶A sites. Renilla luciferase activity was measured and normalized to firefly luciferase activity. *n* = 3 independent biological replicates, and error bars represent standard deviations. Data were compared using Student's *t*-test.
- Q Relative luciferase activities of reporter vectors bearing *IFNAR1*-3' UTR or *IRF3*-5' UTR with wild-type (WT) m⁶A sites after cotransfection with empty vector (EV) or HA-tagged WTAP into shWTAP A549 cells. Renilla luciferase activity was measured and normalized to firefly luciferase activity. *n* = 3 independent biological replicates, and error bars represent standard deviations. Data were compared using Student's *t*-test.

Source data are available online for this figure.

containing wild-type (WT) UTRs (Fig 5P). Moreover, shWTAP A549 cells were cotransfected with reporter constructs bearing WT UTRs of *IRF3* or *IFNAR1* with HA-tagged WTAP and enhanced luciferase activities were obtained (Fig 5Q), indicating that the detected m⁶A sites in *IRF3* and *IFNAR1* transcripts are direct substrates of WTAP. However, using the same approach, we found that METTL3 depletion did not significantly reduce the luciferase activities of the reporter bearing the *IFNAR1*-3' UTR or *IRF3*-5' UTR compared with WTAP depletion. Thus, the ability of WTAP to bring METTL3 to specific m⁶A sites may alter the *IRF3* and *IFNAR1* protein output (Fig EV5H). Taken together, these data suggest that WTAP maintains the expression of *IRF3* by enhancing its translation efficiency via m⁶A modification at its 5'UTR. WTAP also maintains the expression of *IFNAR1* by improving its mRNA stability via m⁶A modification at its 3'UTR.

The protein abundances of IRF3 and IFNAR1 are decreased in virus-infected or nucleic acid analog-treated cells

To further confirm that proteasomal degradation of WTAP can directly result in a decrease in *IRF3* and *IFNAR1*, we first detected the protein abundances of *IRF3* and *IFNAR1* during viral infection or nucleic acid analog stimulation. The results clearly showed decreased protein abundances of *IRF3* and *IFNAR1* in A549 cells stimulated with poly (I:C) or poly (dA:dT) (Fig 6A). Similar results were also obtained in A549 and L929 cells with VSV-eGFP infection (Fig 6B). Then, to show whether the decrease in *IRF3* and *IFNAR1* protein levels is related to translational suppression of *IRF3* and instability of *IFNAR1* mRNA after stimulation, mRNA decay tests

were performed and showed that *IFNAR1* mRNA became more unstable after poly (I:C)-LMW stimulation (Fig 6C) or VSV-eGFP infection (Fig 6D). Polysome profiling assays showed that the distribution of *IRF3*, instead of *IFNAR1* mRNA, shifted to the lighter fraction to a certain degree after poly (I:C)-LMW stimulation (Fig 6E). Next, we transfected 293T cells with a reporter construct bearing the wild-type *IFNAR1*-3' UTR or *IRF3*-5' UTR and found that the luciferase activities of the reporter were much lower after poly (I:C)-LMW stimulation or VSV-eGFP infection (Fig 6F). These results suggest that activation of IFN-I signaling results in reduced translation efficiency of *IRF3* and *IFNAR1* mRNA stability. Moreover, we observed that the protein abundance of *IRF3* and *IFNAR1* decreased faster in shWTAP A549 cells after VSV-eGFP infection (Fig 6G). Therefore, we next performed experiments in the presence of the proteasome inhibitor PR-171 and found that PR-171 can also block the degradation of *IRF3* and *IFNAR1* after poly (I:C)-LMW stimulation or VSV-eGFP infection by restoring the WTAP protein (Fig 6H and I). Thus, all these data suggest that WTAP may maintain the protein abundance of *IRF3* and *IFNAR1* in the resting state. Upon viral infection, degradation of WTAP can reduce the m⁶A modification levels of *IRF3* and *IFNAR1*, providing a fine-tuned mechanism for negative feedback regulation of IFN-I signaling responses.

Discussion

m⁶A is one of the most important posttranscriptional mRNA modifications and regulates RNA splicing, transport, translation, stability,

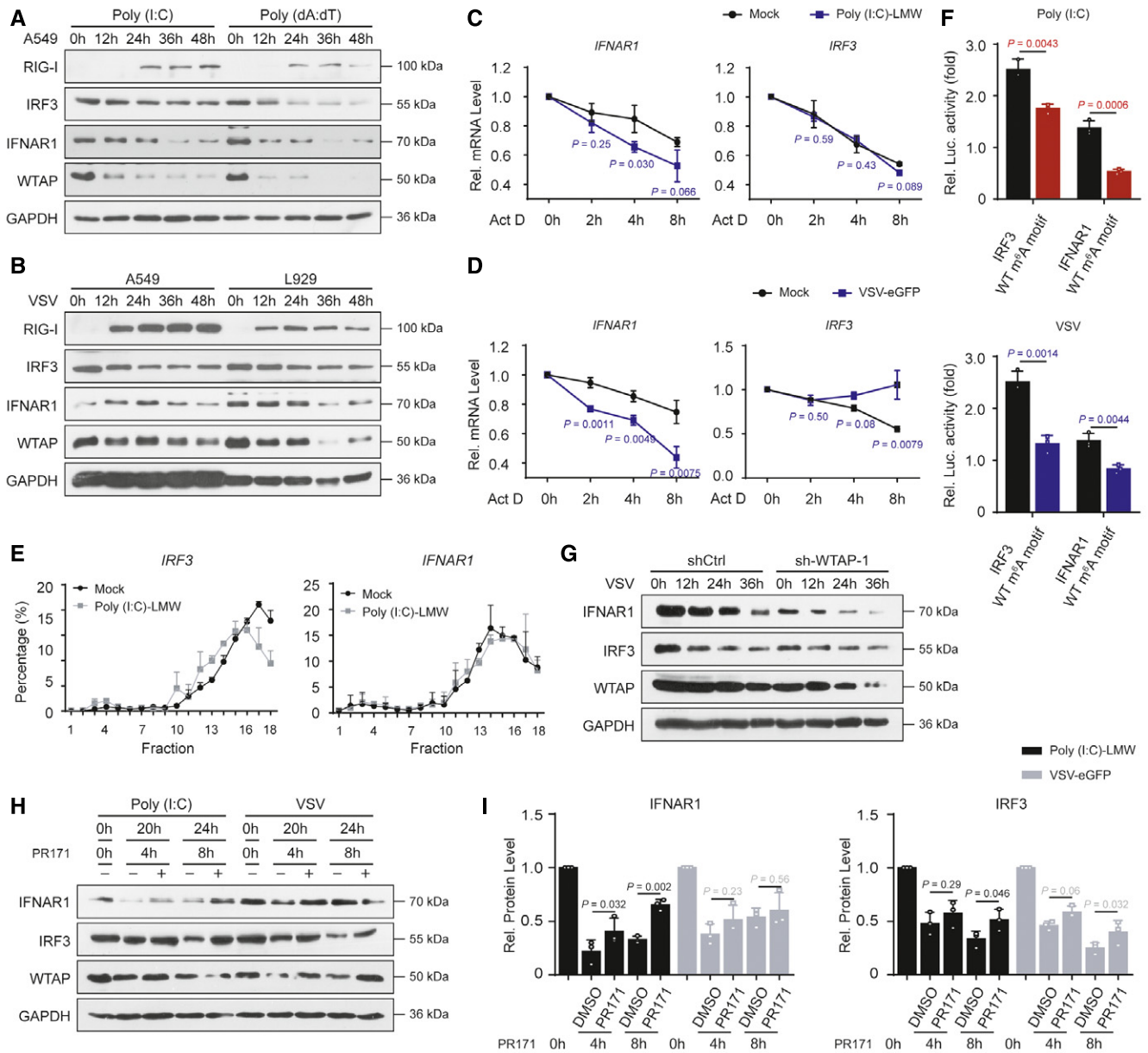


Figure 6. The protein abundances of IRF3 and IFNAR1 are decreased in virus-infected or nucleic acid analog-treated cells.

- A** Immunoblot analyses to detect IRF3 and IFNAR1 protein expression in A549 cells stimulated with poly (I:C) or poly (dA:dT) at the indicated time points. Data are representative of three independent biological experiments.
- B** Immunoblot analyses to detect IRF3 and IFNAR1 protein expression in A549 and L929 cells infected with VSV-eGFP at the indicated time points. Data are representative of three independent biological experiments.
- C, D** qRT-PCR analyses of the mRNA abundance of *IFNAR1* and *IRF3* in A549 cells transfected with poly (I:C)-LMW (**C**) or infected with VSV-eGFP (**D**) for 16 h, followed by treatment with Act D (5 μ g/ml) for the indicated times. $n = 3$ independent biological replicates, and error bars represent standard deviations. Data were compared using Student's *t*-test.
- E** qRT-PCR analyses of the proportion of *IRF3* and *IFNAR1* mRNAs in polysome fractions from A549 cells transfected with poly (I:C)-LMW for 16 h. $n = 3$ independent biological replicates, and error bars represent standard deviations. Data were compared using Student's *t*-test.
- F** Relative luciferase activities of *IFNAR1*-3' UTR or *IRF3*-5' UTR with wild-type (WT) m⁶A sites in 293T cells that were transfected with poly (I:C)-LMW or infected with VSV-eGFP for 24 h. Renilla luciferase activity was measured and normalized to firefly luciferase activity. $n = 3$ independent biological replicates, and error bars represent standard deviations. Data were compared using Student's *t*-test.
- G** Immunoblot analyses of IRF3 and IFNAR1 in shCtrl and shWTAP A549 cells, followed by infection with VSV-eGFP at the indicated time points. Data are representative of three independent biological experiments.
- H, I** Immunoblot analysis of the protein abundance of IRF3 and IFNAR1 in A549 cells transfected with poly (I:C)-LMW or infected with VSV-GFP for 16 h and then treated with PR-171 or DMSO for additional 4 and 8 h. Representative images from three independent biological experiments are shown (**H**), and the relative levels of IFNAR1 (left) and IRF3 (right) are presented as the mean \pm SD (**I**).

Source data are available online for this figure.

and localization. m⁶A is involved in diverse biological processes, including the antiviral immune responses. For example, hnRNP A2B1 can prevent recruitment of the m⁶A eraser FTO to *CGAS*, *IFI16*, and *STING* mRNA, thereby blocking m⁶A removal from these transcripts and enabling their efficient export to amplify antiviral responses (Wang *et al*, 2019); the mRNAs of *IFNA* and *IFNB* are m⁶A-modified and stabilized following depletion of METTL3 or METTL14, leading to increases in IFN-I expression and ISG induction (Winkler *et al*, 2019); m⁶A methylation shields the antigenome and genome of HMPV (human metapneumovirus) from recognition by RIG-I, thereby inhibiting RIG-I-dependent production of type I IFNs in virus-infected cells (Lu *et al*, 2020). In this study, we observed that WTAP, a component of the m⁶A “writer”, is specifically degraded in a ubiquitination-proteasome-dependent manner upon virus and nucleic acid analog-mediated activation of IFN-I signaling. Along with proteasomal degradation of WTAP, the m⁶A modification levels of *IRF3* and *IFNAR1* mRNAs, two critical molecules in IFN-I signaling, were impaired. The decreased m⁶A modification levels resulted in reduced translation efficiency of *IRF3* and instability of *IFNAR1* mRNA, fine-tuning the IFN-I dependent antiviral strategy. Thus, upon viral infection, dynamic m⁶A modifications of specific RNAs involved in multiple antiviral levels may affect the arms race between hosts and pathogens.

As an indispensable transcription factor and a membrane-bound receptor in the IFN-I based antiviral response, the feedback regulation of IFN-I signaling by targeting *IRF3* and *IFNAR1* at the post-translational level has been extensively studied in recent decades. For instance, *IRF3* was found to undergo phosphorylation and ubiquitination-dependent activation. Proteasomal or lysosomal degradation of *IRF3* (Saitoh *et al*, 2006; Higgs *et al*, 2008; Zhang *et al*, 2008; Lei *et al*, 2013; Zhao *et al*, 2016) and *IFNAR1* (Liu *et al*, 2009; Bhattacharya *et al*, 2011; Zheng *et al*, 2011) can result in reduced production of IFN-I and limited activation of the Jak-STAT signaling. Here, we further identified a mechanism that negatively regulates the IFN-I based antiviral response by targeting *IRF3* and *IFNAR1* at the posttranscriptional level, suggesting sophisticated regulation of IFN-I signaling in the host to maintain tissue homeostasis and avoid excessive immune activation.

As methyltransferase, the METTL3/METTL14 heterodimer prefers to recognize RRACH (R = A or G; H = A, C, or U) motifs and transfer a methyl group to adenosine. Since its discovery as an important component of the m⁶A writer, WTAP has been highlighted for tethering the METTL3-METTL14 heterodimers to target RNAs and facilitate their accumulation in nuclear speckles (Zhong *et al*, 2008; Ping *et al*, 2014). Along with providing a novel feedback mechanism in regulation of antiviral responses, we also revealed that some m⁶A modification sites in target genes are WTAP-specific. First, we only observed that the protein abundance of *IRF3* and *IFNAR1* but not that of the other tested proteins was impaired in WTAP deficiency. Second, we found that although the m⁶A methylation levels of *IRF3* and *IFNAR1* could be affected by depletion of both WTAP and METTL3/METTL14, only some site-specific modifications brought by WTAP may alter the subsequent protein outputs. Third, studies by Winkler and Rubio revealed that the m⁶A modification of *IFNB1* mRNA is enhanced in METTL3- or METTL14-silenced cells, resulting in instability of *IFNB1* mRNA and promotion of HCMV replication (Rubio *et al*, 2018; Winkler *et al*, 2019). However, in this study, we found that the stability of *IFNB1*

transcripts was not affected in WTAP knockdown A549 cells (Fig EV5I). Likewise, the fate of *IRF3* and *IFNAR1* transcripts was not affected by METTL3 knockdown (Fig EV5J and K). These observations further indicate a complicated regulatory relationship between m⁶A “Writer” proteins and target genes.

In addition to affecting the fate of certain host immune-related genes, METTL3 deficiency can reduce the replication of HCMV, while WTAP knockdown significantly restrained VSV replication and release (Fig EV5L–O). Meanwhile, lower SeV and HSV-1 mRNA and protein levels were observed in WTAP-silenced A549 cells (Fig EV5O–Q). These data indicate that WTAP can directly regulate viral life cycles in addition to affecting cellular immune responses. From this point of view, whether WTAP negatively regulates the IFN-I signaling by targeting *IRF3* and *IFNAR1* or influences viral replication by acting on viral RNA, the decrease in WTAP protein maintains tissue homeostasis in the host upon viral infection. Thus, painting a more complete picture of the mechanisms by which m⁶A influences viral infection as well as host IFN-I responses will be even more important to address in the future.

Unlike proteasomal degradation upon viral infection, WTAP has been found to be overexpressed and serve as a considerable risk factor in a variety of tumors. For example, WTAP can facilitate hepatocellular carcinoma progression via m⁶A-HuR (Hu-Antigen R)-dependent epigenetic silencing of *ETS1* (Chen *et al*, 2019). It has also been found to promote osteosarcoma tumorigenesis by repressing *HMBOX1* expression in an m⁶A-dependent manner (Chen *et al*, 2020). WTAP can also be upregulated transcriptionally in bacteria-induced inflammatory responses, as well as in HCMV infection (Rubio *et al*, 2018; Wu *et al*, 2020). Thus, the protein abundance of WTAP may be a smart and broad equalizer to regulate multiple biological processes by facilitating the ability of the METTL3-METTL14 heterodimer to target specific genes at specific sites, which may be a very interesting research hotspot of m⁶A modification in the future.

Overall, our study first identified that degradation of WTAP reduces the protein abundance of *IRF3* and *IFNAR1* through m⁶A modification, which not only provides a new negative feedback regulation mechanism to fine-tune the output of IFN-I and ISGs at the posttranscriptional level but also broadens the multilayer regulation of innate immunity, suggesting that such interplay may be essential for novel therapeutic applications in a range of infectious and potentially inflammatory diseases.

Materials and Methods

Cells, reagents, and viruses

293T, A549, L929 cells, and MEFs were grown as a monolayer at 37°C, under 5% CO₂ in DMEM (Thermo Fisher Scientific) supplemented with 10% FBS (Thermo Fisher Scientific) and 1% penicillin/streptomycin. Mouse bone marrow-derived macrophages (BMDMs) were derived from bone marrow of six-week-old female C57BL/6J mice (Guangdong Medical Laboratory Animal Center) and cultured for 6–8 days with 50 ng/ml macrophage colony-stimulating factor (PeproTech). Human peripheral blood mononuclear cells (PBMCs) were isolated from blood of anonymous donors (Zhongshan School of Medicine, Sun Yat-sen University) by density gradient centrifugation using Lymphoprep (AXIS-SHIELD). The source and use of

BMDMs and PBMCs was in compliance with institutional guidelines and approved protocols of Sun Yat-sen University.

Polyinosinic-polycytidylic acid (i.e., poly(I:C)) is a synthetic analog of double-stranded RNA (dsRNA), a molecular pattern which can activate IFN-I response. Poly (deoxyadenylic-deoxythymidylic) acid (i.e., Poly(dA:dT)) is a repetitive synthetic double-stranded DNA sequence of poly(dA-dT):poly(dT-dA) and a synthetic analog of B-DNA. Poly(I:C)-HMW, poly(I:C)-LMW, and poly(dA:dT) were purchased from InvivoGen. Chloroquine (CQ) and bafilomycin A1 (Baf A1) were purchased from Sigma. Carfilzomib (PR-171) and bortezomib (PS-341) were purchased from Selleck. Lipofectamine 3000 and Lipofectamine RNAiMAX were purchased from Invitrogen.

Protein G Sepharose was purchased from GE Healthcare. Anti-RIG-I, MDA5, WTAP, METTL14, MAVS, STING, Ub, STAT1, STAT2, LC3B, phosphorylated TBK1, phosphorylated IRF3, and phosphorylated STAT1 antibodies were purchased from Cell Signaling Technology; anti-MxA, RSAD2, TBK1, MyD88, TRIF, and ICP-27 antibodies were purchased from Abcam; anti-WTAP, METTL3, IRF3, IFNAR1, IFNAR2, GAPDH, ISG15, HA, and Flag antibodies were purchased from Proteintech; anti-IRF3 and MAVS antibodies were purchased from Santa Cruz, anti-VSV-G antibody was purchased from Sigma; anti-SeV antibody was purchased from MBL.

VSV-eGFP, SeV, and HSV-1 were preserved in our laboratory. These viruses were propagated and their titers were determined on Vero cells. Virus titers were measured by means of 50% of the tissue culture's infectious dose (TCID₅₀). Cells were infected at an indicated MOI in serum-free DMEM for 1 h, washed by 1× PBS, and incubated with fresh complete medium for the times shown in the figures.

ELISA assays and quantitative RT-PCR (qRT-PCR)

The concentrations of IFN-β and CCL5 in culture supernatants were measured using kits from R&D Systems, according to the manufacturer's instructions.

Total RNA was extracted from cells using the TRIzol reagent (Roche) according to the manufacturer's instructions. For RT-PCR analyses, cDNA was generated with PrimerScript™ RT reagent Kit with gDNA Eraser (Perfect Real Time) (TaKaRa) and was analyzed by quantitative real-time PCR using the 2×RealStar Green Power Mixture (GenStar). All data were normalized to GAPDH expression. Primer sequences used were as follows:

Human *GAPDH*: Forward 5'-TGTTGCCATCAATGACCCCTT-3', Reverse 5'-CTCCACGACGTACTCAGCG-3';

Mouse *Gapdh*: Forward 5'-TGACCTCAACTACATGGTCTACA-3', Reverse 5'-CTTCCATTCTCGGCCTTG-3';

Human *IFNB*: Forward 5'-GCTTGGATTCTACAAAGAAGCA-3', Reverse 5'-ATAGATGGTCAATGCGGGCTC-3';

Human *RANTES*: Forward 5'-CCAGCAGTCGTCTTTGTAC-3', Reverse 5'-CTCTGGGTTGGCACACTT-3';

Human *DDX58*: Forward 5'-TGTGCTCCTACAGGTTGTGA-3', Reverse 5'-CACTGGGATCTGATTCCGAAAA-3';

Human *ISG15*: Forward 5'-CCGACATCACCCAGAAGATCG-3', Reverse 5'-TTCGTCCGATTTGTCCAGCA-3';

Human *WTAP*: Forward 5'-ACTGGCCTAAGAGAGTCTGAAG-3', Reverse 5'-GTTGCTAGTCGCATTACAAGGA-3';

Mouse *Wtap*: Forward 5'-GAACCTCTTCCATAAAAAGGTCCG-3', Reverse 5'-TTAACTCATCCCGTGCATAAC-3';

Human *METTL3*: Forward 5'-TTGTCTCCAACCTTCCGTAGT-3', Reverse 5'-CCAGATCAGAGAGGTGGTGTAG-3';

Mouse *Mettl3*: Forward 5'-CTGGGCACTTGGATTTAAGGAA-3', Reverse 5'-TGAGAGGTGGTGTAGCAACTT-3';

Human *METTL14*: Forward 5'-AGTGCCGACAGCATTGGTG-3', Reverse 5'-GGAGCAGAGGTATCATAGGAAGC-3';

Mouse *Mettl14*: Forward 5'-CTGAGAGTGCCGATAGCATTG-3', Reverse 5'-GAGCAGATGTATCATAGGAAGCC-3';

Human *IRF3*: Forward 5'-AGAGGCTCGTGATGGTCAAG-3', Reverse 5'-AGGTCCACAGTATTCTCCAGG-3';

Human *IRF3*-m⁶A site 1: Forward 5'-CCATCGGCTTTTGGTCTGTGTT-3', Reverse 5'-GGATCCGTGGCTTTGGGGTT-3';

Human *IRF3*-m⁶A site 2: Forward 5'-GATCCTGCCCTGGCTGGT-3', Reverse 5'-TTCCGAAATCCTCTGCTGT-3';

Human *IFNAR1*: Forward 5'-ATTTACACCATTTCCGAAAGCTC-3', Reverse 5'-TCCAAAGCCACATAACACTATC-3';

Human *IFNAR1*-m⁶A site 1: Forward 5'-GTTCCCAAACACTGCCAAGA-3', Reverse 5'-CCTCAGGCTCCCAGTGTA-3';

Human *IFNAR1*-m⁶A site 2: Forward 5'-GCCAACGTGGTGAAACCC-3', Reverse 5'-CACATGGAAAAGAATGTAGGA-3'.

VSV-G: Forward 5'-CAAGTCAAATGCCCAAGAGTCACA-3', Reverse 5'-TTTCCTTGCATTGTCTACAGATGG-3';

SeV: Forward 5'-GCTTACGGGACAGATGAGAT-3', Reverse 5'-ATTGTTATGAACCGACTTGC-3';

HSV-1: Forward 5'-TTTCTCCAGTGCTACCTGAAGG-3', Reverse 5'-TCAACTCGCAGACAGACTCG-3'.

Quantification of the m⁶A modification

Total RNA was isolated using TRIzol (Roche) according to the manufacturer's instructions and treated with deoxyribonuclease I (Sigma-Aldrich). RNA quality was analyzed using a NanoDrop. The change of global m⁶A levels in mRNA was measured by EpiQuik m⁶A RNA Methylation Quantification Kit (colorimetric; EpiGenetek) following the manufacturer's protocol. Poly-A-purified RNA (200 ng) was used for each sample analysis. Briefly, 200 ng RNAs were coated on assay wells. Capture antibody solution and detection antibody solution were then added to assay wells separately in a suitable diluted concentration. The m⁶A levels were colorimetrically quantified by reading the absorbance at a wavelength of 450 nm, and then, calculations were performed based on the standard curve.

m⁶A RNA-IP-qRT-PCR (MeRIP-qPCR)

To examine m⁶A modifications in individual genes, the Magna MeRIP m⁶A Kit (Millipore) was used according to the manufacturer's instructions. Briefly, 200 μg of total RNA was sheared to approximately 100 nt in length by metal-ion induced fragmentation and purified, then incubated with m⁶A antibody- or mouse IgG-conjugated Protein A/G Magnetic Beads in 500 μl 1× IP buffer supplemented with RNase inhibitors at 4°C overnight. Methylated RNAs were immunoprecipitated with beads, eluted by competition with free m⁶A, and recovered with the Rneasy kit (QIAGEN). One-tenth of fragmented RNA was saved as input control and further analyzed by qPCR along with the MeRIPed RNAs using primers of targeted gene. The related enrichment of m⁶A in each sample was calculated by normalizing the value of amplification cycle (Cq) of the m⁶A-IP portion to the Cq of the corresponding input proportion.

RNA interference

LipoRNAiMAX (Invitrogen) was used for transfection of siRNAs (30 nM) into A549 cells according to the manufacturer's instructions. The sequences of siRNAs are as follows:

Human WTAP-siRNA-1: AAGGTTTCGATTGAGTGAAACA
 Human WTAP-siRNA-2: GAAGCATATGTACAAGCTT
 Human METTL3-siRNA-1: CTGCAAGTATGTTCACTATGA
 Human METTL3-siRNA-2: CGTCAGTATCTTGGGCAAGTT
 Human METTL14-siRNA-1: GCATTGGTGCCGTGTTAAA
 Human METTL14-siRNA-2: GCAGCACCTCGATCATTTA

Coimmunoprecipitation and immunoblot analysis

Cells were lysed with cell lysis buffer (Cell Signaling Technology) supplemented with protease inhibitor "cocktail" (Roche). Protein concentrations in the extracts were measured by BCA assay (Pierce). Overall, 40 µg proteins were separated by sodium dodecyl sulfate–polyacrylamide gel electrophoresis (SDS–PAGE) followed by electrotransfer to polyvinylidene difluoride membrane (Hybond-P; GE Healthcare Life Sciences). Membranes were probed using indicated antibodies against targeted proteins, followed by the HRP-conjugated second antibody (Cell Signaling Technology, 1:10,000). Bands were revealed with Immobilon ECL kit (Millipore) and recorded on X-ray films (Kodak, Xiamen, China).

Analysis of IRF3 dimerization by native-PAGE

Native-PAGE was performed based on the previously reported protocol (Robitaille *et al*, 2016). The native-PAGE gel was pre-run with 25 mM Tris and 192 mM glycine, PH 8.4 with and without 1% deoxycholate (DOC) in cathode, and anode chamber, respectively, for 30 min at 40 mA. Samples in native sample buffer (10–40 µg protein, 62.5 mM Tris–HCl, PH 6.8, 15% glycerol, and 1% deoxycholate) were applied to the gel and electrophoresed for 60 min at 25 mA. Detailed operating instructions can be found online at <https://www.jove.com/video/53723>.

Polysome profiling

Polysome fractionation was performed based on the previously reported protocol (Gandin *et al*, 2014). Briefly, cells were treated for 15 min with cycloheximide at a final concentration of 100 µg/ml and then lysed with hypotonic buffer (5 mM Tris–HCl, pH 7.5, 2.5 mM MgCl₂, 1.5 mM KCl, 100 µg/ml cyclohexane (CHX), 2 mM DTT, 0.5% Triton X-100, 0.5% sodium deoxycholate, 1× protease inhibitor cocktail [EDTA-free] and 2 units/µL RNase inhibitor). Cytosolic extracts were ultracentrifuged with a 10–45% sucrose gradient buffer (200 mM HEPES, pH 7.6, 1 M KCl, 50 mM MgCl₂, 100 µg/ml cycloheximide, 1× protease inhibitor cocktail [EDTA-free], 100 units/ml RNase inhibitor) prepared using the Gradient Station (Biocomp). Fractions were collected with the Gradient Station. We then merged them into polysome-bound and polysome-unbound fractions based on the OD254 values. Total RNA for each merged fraction was extracted using the TRIzol reagent (Roche) and maintained at equal volumes of RNase-free water. In order to eliminate the interference of RNA loss during the purification step, we extracted the polysome fraction samples spiked with equivalent

RNA probe to normalize the loss of total mRNA. The quality of samples was checked with agarose gel electrophoresis and the OD260/280 ratios.

Luciferase reporter gene assay

Wild-type and WTAP^{-/-} 293T cells, or shNC and shWTAP A549 cells were plated in 48-well plates and transfected with indicated reporter vectors expressing wild-type or mutated UTRs of IFNAR1 or IRF3 using Lipofectamine 2000. At 24 h post-transfection, cells were stimulated with 1 µg/ml poly(I:C) or infected with the indicated dose of VSV-eGFP. Cells were harvested 24 h after stimulation or infection, and luciferase activities were measured with a dual-luciferase reporter assay system (Promega) according to the manufacturer's instructions. Reporter gene activity was determined by normalization of the Renilla luciferase activity to firefly luciferase activity.

Statistical analyses

Data are represented as mean ± SD unless otherwise indicated, and Student's *t*-test was used for all statistical analyses with the GraphPad Prism 5 software. Differences between two groups were considered significant when *P* value was less than 0.05.

Data availability

No primary datasets have been generated and deposited.

Expanded View for this article is available online.

Acknowledgements

We thank Prof. Guanzheng Luo and Mr. Biaodi Liu from Sun Yat-Sen University for their help in data analysis of GSE55572. This work was supported by projects from National Natural Science Foundation of China (91942301, 31770943, 31970852), Ministry of Science and Technology of the People's Republic of China (2018YFD0900502), Guangdong Science and Technology Department (2017B030314021), and Innovation Group Project of Southern Marine Science and Engineering Guangdong Laboratory (Zhuhai) (311021006).

Author contributions

YG, SY, and AX designed the study; YG, TL, YW, XJ, XX, RC, and SC performed the experiments. YG and SY analyzed data and prepared the manuscript. AX and SY conceived the study, led the project, supervised experiments, and wrote the paper.

Conflict of interest

The authors declare that they have no conflict of interest.

References

- Barrat FJ, Crow MK, Ivashkiv LB (2019) Interferon target-gene expression and epigenomic signatures in health and disease. *Nat Immunol* 20: 1574–1583
- Bhattacharya S, Qian J, Tzimas C, Baker DP, Koumenis C, Diehl JA, Fuchs SY (2011) Role of p38 protein kinase in the ligand-independent ubiquitination and down-regulation of the IFNAR1 chain of type I interferon receptor. *J Biol Chem* 286: 22069–22076

- Chelmicki T, Roger E, Teissandier A, Dura M, Bonneville L, Rucli S, Dossin F, Fouassier C, Lameiras S, Bourc'his D (2021) m⁶A RNA methylation regulates the fate of endogenous retroviruses. *Nature* 591: 312–316
- Chen S, Li Y, Zhi S, Ding Z, Wang W, Peng Yi, Huang Y, Zheng R, Yu H, Wang J et al (2020) WTAP promotes osteosarcoma tumorigenesis by repressing HMBOX1 expression in an m⁶A-dependent manner. *Cell Death Dis* 11: 659
- Chen X, Chen Y (2019) Ubiquitination of cGAS by TRAF6 regulates anti-DNA viral innate immune responses. *Biochem Biophys Res Commun* 514: 659–664
- Chen Y, Peng C, Chen J, Chen D, Yang B, He B, Hu W, Zhang Y, Liu H, Dai L et al (2019) WTAP facilitates progression of hepatocellular carcinoma via m⁶A-HuR-dependent epigenetic silencing of ETS1. *Mol Cancer* 18: 127
- Colina R, Costa-Mattoli M, Dowling RJO, Jaramillo M, Tai L-H, Breitbach CJ, Martineau Y, Larsson O, Rong L, Svitkin YV et al (2008) Translational control of the innate immune response through IRF-7. *Nature* 452: 323–328
- Du Y, Hou G, Zhang H, Dou J, He J, Guo Y, Li L, Chen R, Wang Y, Deng R et al (2018) SUMOylation of the m⁶A-RNA methyltransferase METTL3 modulates its function. *Nucleic Acids Res* 46: 5195–5208
- Fricker LD (2020) Proteasome inhibitor drugs. *Annu Rev Pharmacol Toxicol* 60: 457–476
- Frye M, Harada BT, Behm M, He C (2018) RNA modifications modulate gene expression during development. *Science* 361: 1346–1349
- Fustin JM, Kojima R, Itoh K, Chang HY, Ye SQ, Zhuang B, Oji A, Gibo S, Narasimamurthy R, Virshup D et al (2018) Two Ckl delta transcripts regulated by m⁶A methylation code for two antagonistic kinases in the control of the circadian clock. *Proc Natl Acad Sci USA* 115: 5980–5985
- Gack MU, Shin YC, Joo C-H, Urano T, Liang C, Sun L, Takeuchi O, Akira S, Chen Z, Inoue S et al (2007) TRIM25 RING-finger E3 ubiquitin ligase is essential for RIG-I-mediated antiviral activity. *Nature* 446: 916–920
- Gandin V, Sikström K, Alain T, Morita M, McLaughlan S, Larsson O, Topisirovic I (2014) Polysome fractionation and analysis of mammalian translational complexes on a genome-wide scale. *J Vis Exp* 87: 51455
- Higgs R, Ní Gabhann J, Ben Larbi N, Breen EP, Fitzgerald KA, Jefferies CA (2008) The E3 ubiquitin ligase Ro52 negatively regulates IFN-beta production post-pathogen recognition by polyubiquitin-mediated degradation of IRF3. *J Immunol* 181: 1780–1786
- Kato H, Takeuchi O, Sato S, Yoneyama M, Yamamoto M, Matsui K, Uematsu S, Jung A, Kawai T, Ishii KJ et al (2006) Differential roles of MDA5 and RIG-I helicases in the recognition of RNA viruses. *Nature* 441: 101–105
- Kuai Y, Gong X, Ding L, Li F, Lei L, Gong Y, Liu Q, Tan H, Zhang X, Liu D et al (2018) Wilms' tumor 1-associating protein plays an aggressive role in diffuse large B-cell lymphoma and forms a complex with BCL6 via Hsp90. *Cell Commun Signal* 16: 50
- Lei CQ, Zhang Y, Xia T, Jiang LQ, Zhong B, Shu HB (2013) FoxO1 negatively regulates cellular antiviral response by promoting degradation of IRF3. *J Biol Chem* 288: 12596–12604
- Levy DE, Kessler DS, Pine R, Reich N, Darnell Jr JE (1988) Interferon-induced nuclear factors that bind a shared promoter element correlate with positive and negative transcriptional control. *Genes Dev* 2: 383–393
- Liu J, HuangFu WC, Kumar KG, Qian J, Casey JP, Hamanaka RB, Grigoriadou C, Aldabe R, Diehl JA, Fuchs SY (2009) Virus-induced unfolded protein response attenuates antiviral defenses via phosphorylation-dependent degradation of the type I interferon receptor. *Cell host microbe* 5: 72–83
- Liu S, Cai X, Wu J, Cong Q, Chen X, Li T, Du F, Ren J, Wu Y-T, Grishin NV et al (2015) Phosphorylation of innate immune adaptor proteins MAVS, STING, and TRIF induces IRF3 activation. *Science* 347: aaa2630
- Lu M, Zhang Z, Xue M, Zhao BS, Harder O, Li A, Liang X, Gao TZ, Xu Y, Zhou J et al (2020) N⁶-methyladenosine modification enables viral RNA to escape recognition by RNA sensor RIG-I. *Nat Microbiol* 5: 584–598
- Meyer KD, Jaffrey SR (2017) Rethinking m⁶A readers, writers, and erasers. *Annu Rev Cell Dev Biol* 33: 319–342
- Ping X-L, Sun B-F, Wang LU, Xiao W, Yang X, Wang W-J, Adhikari S, Shi Y, Lv Y, Chen Y-S et al (2014) Mammalian WTAP is a regulatory subunit of the RNA N⁶-methyladenosine methyltransferase. *Cell Res* 24: 177–189
- Ran FA, Hsu PD, Wright J, Agarwala V, Scott DA, Zhang F (2013) Genome engineering using the CRISPR-Cas9 system. *Nat Protoc* 8: 2281–2308
- Robitaille AC, Mariani MK, Fortin A, Grandvaux N (2016) A high resolution method to monitor phosphorylation-dependent activation of IRF3. *J Vis Exp* 107: e53723
- Roignant JY, Soller M (2017) m⁶A in mRNA: an ancient mechanism for fine-tuning gene expression. *Trends Genet* 33: 380–390
- Roundtree IA, Evans ME, Pan T, He C (2017) Dynamic RNA modifications in gene expression regulation. *Cell* 169: 1187–1200
- Rubio RM, Depledge DP, Bianco C, Thompson L, Mohr I (2018) RNA m⁶A modification enzymes shape innate responses to DNA by regulating interferon beta. *Genes Dev* 32: 1472–1484
- Saitoh T, Tun-Kyi A, Ryo A, Yamamoto M, Finn G, Fujita T, Akira S, Yamamoto N, Lu KP, Yamaoka S (2006) Negative regulation of interferon-regulatory factor 3-dependent innate antiviral response by the prolyl isomerase Pin1. *Nat Immunol* 7: 598–605
- Schlee M, Hartmann G (2016) Discriminating self from non-self in nucleic acid sensing. *Nat Rev Immunol* 16: 566–580
- Schneider WM, Chevillotte MD, Rice CM (2014) Interferon-stimulated genes: a complex web of host defenses. *Annu Rev Immunol* 32: 513–545
- Schwartz S, Mumbach MR, Jovanovic M, Wang T, Maciag K, Bushkin GG, Mertins P, Ter-Ovanesyan D, Habib N, & Cacchiarelli D et al (2014) Gene expression Omnibus GSE 55572 (<https://www.ncbi.nlm.nih.gov/geo/query/acc.cgi?acc=GSE55572>). [DATASET]
- Śledź P, Jinek M (2016) Structural insights into the molecular mechanism of the m⁶A writer complex. *eLife* 5: e18434
- Tao X, Chu B, Xin D, Li L, Sun Q (2020) USP27X negatively regulates antiviral signaling by deubiquitinating RIG-I. *PLoS Pathog* 16: e1008293
- Villarino AV, Kanno Y, O'Shea JJ (2017) Mechanisms and consequences of Jak-STAT signaling in the immune system. *Nat Immunol* 18: 374–384
- Wang X, Lu Z, Gomez A, Hon GC, Yue Y, Han D, Fu Y, Parisien M, Dai Q, Jia G et al (2014) N⁶-methyladenosine-dependent regulation of messenger RNA stability. *Nature* 505: 117–120
- Wang X, Zhao BS, Roundtree IA, Lu Z, Han D, Ma H, Weng X, Chen K, Shi H, He C (2015) N(6)-methyladenosine modulates messenger RNA translation efficiency. *Cell* 161: 1388–1399
- Wang X, Feng J, Xue Y, Guan Z, Zhang D, Liu Z, Gong Z, Wang Q, Huang J, Tang C et al (2016) Structural basis of N(6)-adenosine methylation by the METTL3-METTL14 complex. *Nature* 534: 575–578
- Wang L, Wen M, Cao X (2019) Nuclear hnRNP2B1 initiates and amplifies the innate immune response to DNA viruses. *Science* 365: eaav0758
- Winkler R, Gillis E, Lasman L, Safra M, Geula S, Soyris C, Nachshon A, Tai-Schmiedel J, Friedman N, Le-Trilling VTK et al (2019) m⁶A modification controls the innate immune response to infection by targeting type I interferons. *Nat Immunol* 20: 173–182
- Wu C, Chen W, He J, Jin S, Liu Y, Yi Y, Gao Z, Yang J, Yang J, Cui J et al (2020) Interplay of m⁶A and H3K27 trimethylation restrains inflammation during bacterial infection. *Sci Adv* 6: eaba0647
- Xiang Y, Laurent B, Hsu C-H, Nachtergaele S, Lu Z, Sheng W, Xu C, Chen H, Ouyang J, Wang S et al (2017) RNA m⁶A methylation regulates the ultraviolet-induced DNA damage response. *Nature* 543: 573–576

- Xu K, Yang Y, Feng G-H, Sun B-F, Chen J-Q, Li Y-F, Chen Y-S, Zhang X-X, Wang C-X, Jiang L-Y et al (2017) Mettl3-mediated m⁶A regulates spermatogonial differentiation and meiosis initiation. *Cell Res* 27: 1100–1114
- Xuan JJ, Sun WJ, Lin PH, Zhou KR, Liu S, Zheng LL, Qu LH, Yang JH (2018) RMBase v2.0: deciphering the map of RNA modifications from epitranscriptome sequencing data. *Nucleic Acids Res* 46: D327–D334
- Yan N, Chen ZJ (2012) Intrinsic antiviral immunity. *Nat Immunol* 13: 214–222
- Zhang M, Tian Y, Wang RP, Gao D, Zhang Y, Diao FC, Chen DY, Zhai ZH, Shu HB (2008) Negative feedback regulation of cellular antiviral signaling by RBCK1-mediated degradation of IRF3. *Cell Res* 18: 1096–1104
- Zhang Q, Tang Z, An R, Ye L, Zhong B (2020) USP29 maintains the stability of cGAS and promotes cellular antiviral responses and autoimmunity. *Cell Res* 30: 914–927
- Zhao X, Zhu H, Yu J, Li H, Ge J, Chen W (2016) c-Cbl-mediated ubiquitination of IRF3 negatively regulates IFN-beta production and cellular antiviral response. *Cell Signal* 28: 1683–1693
- Zheng H, Qian J, Varghese B, Baker DP, Fuchs S (2011) Ligand-stimulated downregulation of the alpha interferon receptor: role of protein kinase D2. *Mol Cell Biol* 31: 710–720
- Zheng Q, Hou J, Zhou Y, Li Z, Cao X (2017) The RNA helicase DDX46 inhibits innate immunity by entrapping m⁶A-demethylated antiviral transcripts in the nucleus. *Nat Immunol* 18: 1094–1103
- Zhong S, Li H, Bodi Z, Button J, Vespa L, Herzog M, Fray RG (2008) MTA is an Arabidopsis messenger RNA adenosine methylase and interacts with a homolog of a sex-specific splicing factor. *Plant Cell* 20: 1278–1288
- Zhou J, Wan J, Shu XE, Mao Y, Liu XM, Yuan X, Zhang X, Hess ME, Brüning JC, Qian SB (2018) N(6)-methyladenosine guides mRNA alternative translation during integrated stress response. *Mol Cell* 69: 636–647



License: This is an open access article under the terms of the Creative Commons Attribution-NonCommercial-NoDerivs License, which permits use and distribution in any medium, provided the original work is properly cited, the use is non-commercial and no modifications or adaptations are made.